Available online at www.sciencedirect.com
SCIENCE DIRECT®
Journal of Chromatography A, 1068 (2005) 261–268
JOURNAL OF CHROMATOGRAPHY A
www.elsevier.com/locate/chroma

# Elimination of edge effects in micro-thermal field-flow fractionation channel of low aspect ratio by splitting the carrier liquid flow into the main central stream and the thin stream layers at the side channel walls

Josef Janča [a,*], Jan Dupák [b]

[a] *Université de La Rochelle, Pôle Sciences et Technologie, Avenue Michel Crépeau, 17042 La Rochelle Cedex 01, France*
[b] *Institute of Scientific Instruments, Academy of Sciences of the Czech Republic, Královopolská 147, 61264 Brno, Czech Republic*

Received 20 November 2004; received in revised form 18 January 2005; accepted 28 January 2005

**Abstract**

An optimized construction of the separation channel for micro-thermal field-flow fractionation (FFF) was proposed and studied experimentally. The sample is injected in such a manner that its zone moves along the channel only in the main central stream where the flow velocity profile in the plane parallel to the main accumulation wall is practically flat. This central stream is separated from the contact with the side walls of the channel by thin flowing layers of the free carrier liquid. The retained species do not reach the thin liquid streams at the side walls where the flow rate decreases rapidly to achieve zero at the side wall according to the established 3D flow velocity profile. Such a construction of the channel allows one to reduce the aspect ratio (the ratio of the channel breadth $b$ to its thickness $w$) without increasing the zone broadening. The hydrodynamic splitting of the outlet streams allows one not only to increase the concentration of the detected species but also the determination of the sign of Soret coefficient.


*Keywords:* Micro-thermal field-flow fractionation; Edge effects; Inlet and outlet hydrodynamic splitting; New injection mode

## 1. Introduction

The separation in field-flow fractionation (FFF) is generally driven by one of three basic mechanisms: *polarization*, *steric*, *and focusing*. In order to achieve high-performance separations, the experiments must usually be performed under the conditions of one dominating mechanism. A high versatility and an extended range of the operational variables that can be controlled are the factors that allow one to impose the most convenient mechanism, operating under the optimized experimental conditions. Such optimal conditions can be achieved with micro-thermal field-flow fractionation (micro-TFFF), invented and developed recently [1]. An extended range of the controlled operational variables in micro-TFFF is a consequence of a highly reduced total heat flow across the miniaturized channel (10–20 times in comparison with standard size channels). A detailed theoretical analysis and the related experimental studies of various aspects and advantages of the miniaturization of TFFF with respect to the high-resolution separation and easy manipulation of the operational parameters were published recently [2].

The separation channel for TFFF is usually constructed as shown schematically in a 3D representation in Fig. 1, where $L$ is the length, $w$ is the thickness, and $b$ is the breadth. The idea of miniaturization of TFFF channel is thus related with the question: Which of the three channel dimensions can usefully be reduced?

The crucial advantage of the miniaturization of TFFF channel follows from the theory which predicts [1] that the

* Corresponding author. Tel.: +33 5 46458218; fax: +33 5 46421242.
*E-mail address:* jjanca@univ-lr.fr (J. Janča).

0021-9673/$ – see front matter © 2005 Elsevier B.V. All rights reserved.
doi:10.1016/j.chroma.2005.01.078

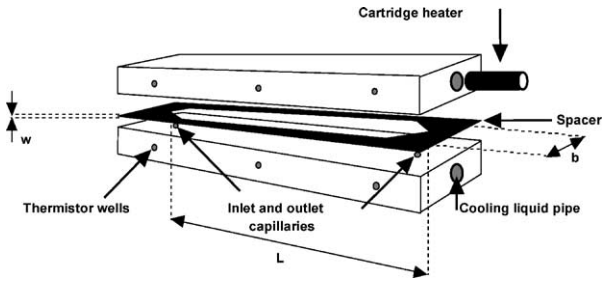


Fig. 1. Schematic representation of thermal field-flow fractionation channel.

resolution can conveniently be manipulated according to the relationship:

$$R_s = \left(\frac{1}{8w}\right)\sqrt{\frac{L D_T^3 \Delta T^3}{6\langle v\rangle}}\left|\frac{1}{D_1} - \frac{1}{D_2}\right| \quad (1)$$

The $D_{1,2}$ in Eq. (1) are the diffusion coefficients of the two resolved species of different molar masses or particle sizes, $D_T$ is the thermal diffusion coefficient of these species supposed to be identical for both of them, and $\Delta T$ is the temperature drop across the channel thickness.

The Eq. (1) shows that the shortening of the channel length $L$ accompanied by the proportional decrease in the mean linear velocity $\langle v\rangle$ of the carrier liquid keeps the resolution unchanged. The immediate gain, however, is that the total heat flow across the channel is reduced proportionally to the shortening of the length of the channel. The reduced heat flow makes the control of the temperatures much easier and, more importantly, according to Fourier's law of heat conduction, it allows to extend the range of the temperature drops $\Delta T$ that can be achieved.

When decreasing $w$, $\Delta T$ must not change (in order to keep the retentions and thus the resolution unchanged) which means that the total heat flow across the channel increases proportionally. On the other hand, an advantage which follows from the Eq. (1) is that an increase in $\Delta T$ has a more important impact on the resolution than a proportional decrease in $w$ for the same increase in total heat flow across the channel. Consequently, an increase in resolution can be more efficiently achieved by increasing $\Delta T$ than by reducing $w$. This is very important theoretical finding [1] which has been proven experimentally [3]. Moreover, the reduced thickness of the channel complicates the separation of large size species due to the possible simultaneous intervention of the polarization and steric exclusion mechanisms [4,5]. When decreasing $w$, the effect of steric exclusion starts at smaller size of the retained species or, in other words, the inversion point is shifted to smaller species. In such a case, the resolution is deteriorated and may even reach zero at the inversion point where the order of elution changes and the separation mechanism passes from polarization to steric one. As a result, it is obvious that a decrease in channel thickness $w$ does not represent an advantageous solution and that this dimension should not be reduced under an optimum when miniaturizing the TFFF channel. Such an optimum should take into account namely the acceptable total heat flow across the channel, imposed by the technical limits of the available refrigerated thermostats, and a reasonable time of analysis determined also by casual stop-flow time for relaxation, discussed briefly in the following paragraph.

On the other hand, an increase in $w$ does not lead to an advantageous extension of the range of particle sizes which could effectively be separated in steric mode. For a channel of standard construction, such an increase should be accompanied by an increase in channel breadth $b$, in order to keep the aspect ratio $b/w$ constant, otherwise the efficiency, described by the number of theoretical plates, decreases [6–8]. If the channel thickness $w$ is increased without increasing proportionally the breadth $b$, a decrease in efficiency is caused by a proportionally increased contribution to the band broadening due to the retained species eluting in the layers adjoined to the side walls of the channel. The linear velocity of the carrier liquid strongly decreases in these layers to achieve zero at the side walls in agreement with the established 3D flow velocity profile [9], shown schematically in Fig. 2. The mass transfer in the plane parallel to the accumulation wall thus contributes to an increase in band broadening. The resolution decreases consequently with a reduced aspect ratio as demonstrated recently [5]. Moreover, an increase in $w$ imposes the increase

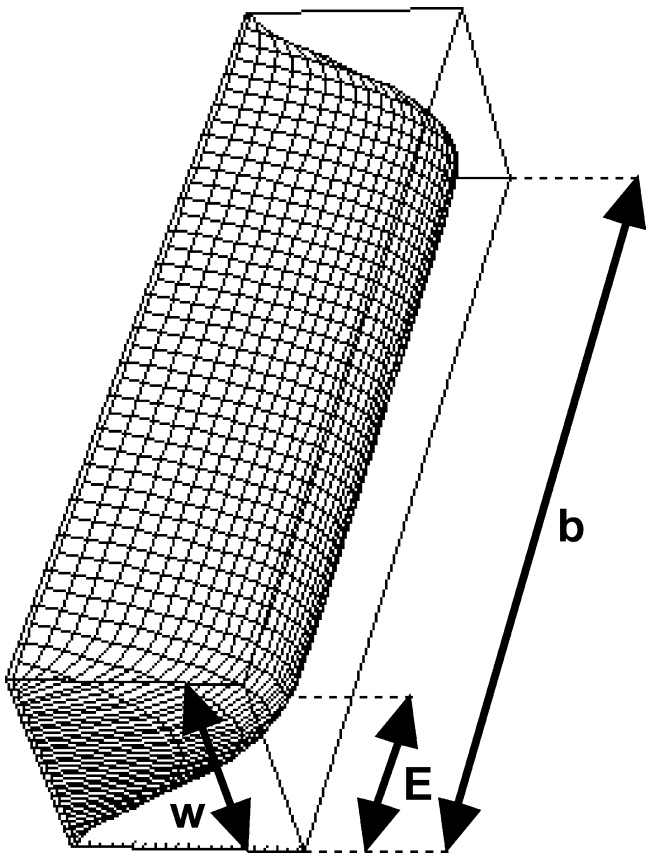


Fig. 2. Schematic representation of three-dimensional flow velocity profile established in rectangular cross-section channel: $b$ = channel breadth, $w$ = channel thickness, $E$ = edge zone layer.

in stop-flow time for relaxation just after the injection of the sample. Such a procedure is necessary in some cases in order to achieve high-performance separation. Since the relaxation time and, consequently the stop-flow time, is proportional to the $w^2$ [10], the resulting increase in total analysis time may be important and unacceptable.

The authors of the crucial papers [6–8] dealing with the band broadening and efficiency in rectangular cross-section channel (a typical shape of a FFF channel) concluded that an optimal aspect ratio, $a$, should be $a = b/w > 100$. The only different alternative was described by Golay [6] who proposed to modify the rectangular cross-section channel by terminating both ends of the rectangular cross-section with enlarged circular portion with a diameter of approximately one and a half times the thickness of the channel so as to have a carrier liquid flow near the end equal, on an average, to the average flow in the entire channel. Nevertheless, already Golay [6] recognized that such a construction would be very difficult to realize.

Our idea to modify the injection mode by the hydrodynamic splitting of the carrier liquid flow into the main central stream and two thin stream layers at the side walls of the channel is based on our former experimental findings that the purely diffusive mixing between the adjoined streamlines flowing under the laminar conditions was practically negligible in focusing FFF experiments [11,12]. The non-mixing conditions in our former experiments [11,12] were due to a step density gradient formed vertically inside the separation channel and stabilized by the gravitation.

In order to eliminate the edge effects in micro-TFFF channel, the splitting of the carrier liquid into the main central layer and two thin side layers is carried out in horizontal plane. The absence of the hydrodynamic instabilities together with an optimized splitting ratio restricts the diffusive transport of the retained species from the central stream to the thin carrier liquid layers at the channel edges. Thus the band broadening due to the low aspect ratio $a = b/w$ of a miniaturized TFFF channel can substantially be reduced to a negligible contribution. In a theoretical analysis of edge effects, Giddings and Schure [13] mentioned a possibility to confine the sample to the central region of the channel by a sheath of pure carrier liquid, the idea already proposed in 1977 [14], but they considered an experimental realization as difficult. As a result, such a channel design was never realized. The injection of the sample through a septum (manually by using a micro-syringe) in the center of the channel downstream from the flow inlet can partly eliminate the edge effects [14]. The problem is that this mode of injection makes the control of the ratio of the speed of injection to the velocity of the carrier liquid practically impossible. Consequently, it is impossible to control whether the zone of the injected sample reaches the channel edges at different carrier liquid flow rates or not. On the other hand, the above proposed injection mode by the hydrodynamic splitting of the carrier liquid flow and the use of the injection valve makes the injection procedure perfectly controllable and reproducible.

The above-mentioned theoretical findings raise the question where is the lower limit of the miniaturization of the channel. It can be found by considering the efficiency of FFF [1], which is described by the height equivalent to the theoretical plate $H$:

$$H = \frac{2D}{R\langle v\rangle} + \frac{\chi w^2 \langle v\rangle}{D} + \sum H_i \tag{2}$$

where $R$ is the retention ratio, the sum of $H_i$ represents mainly the extra-channel contributions to the plate height which can be reduced to negligible minimum [1], and $\chi$ is a dimensionless parameter which for highly retained species can be approximated by:

$$\lim_{R\to 0} \chi = \frac{R^3}{9} \tag{3}$$

The first term in Eq. (2) describes the longitudinal diffusion and the second one corresponds to the nonequilibrium (mass transfer) processes. As the diffusion coefficients of the macromolecules or particles are very low, the lower limit of $\langle v\rangle$ calculated from the Eq. (2) is roughly $\langle v\rangle = 10^{-3}$ mm/s [1].

## 2. Experimental

The experimental setup for micro-TFFF consisted of a syringe pump model IPC 2050 (Linet Compact, Czech Republic), a compact and versatile micro-TFFF channel unit described in detail in the following paragraphs, a UV–vis variable wavelength detector model LCD 5000 (Ingos, Czech Republic) equipped with the 1 μl cell, low temperature thermostat model RML 6 B (Lauda, Germany) controlling the temperature of the cold wall of the channel, and an electronic device regulating the electric power for heating cartridge and controlling the temperature of the hot wall, designed and constructed in our laboratory. The temperatures at very close proximities of the cold and hot walls were measured also independently by digital thermometer (Hanna Instruments, Portugal) equipped with two thermocouples. The digital data from the UV–vis detector were acquisitioned with a PC by using CHROMuLAN software (PiKron, Czech Republic).

The compact and versatile micro-TFFF channel unit was designed and assembled by MicroFrac Laboratory (microfrac@atlas.cz, Czech Republic). The central part of this unit, the separation micro-channel, was designed in our laboratory and fabricated by the Institute of Scientific Instruments (Academy of Sciences of the Czech Republic). The thickness of the micro-TFFF channel $w$ can easily be changed according to the requirements of the experiment and the channel can be operated either in horizontal or exactly defined inclined position allowing various studies of thermal diffusion of polymers and colloidal particles. The dimensions of the micro-TFFF channel used in this work were 0.1 mm × 3.2 mm × 76 mm. The compact micro-TFFF unit was further equipped with an injection valve model 7410

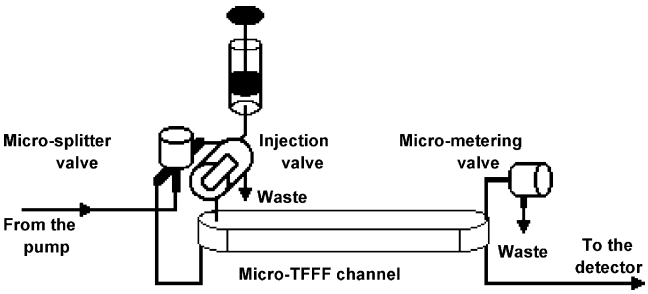


Fig. 3. Schematic representation of micro-thermal field-flow fractionation unit.

Table 1
Particle size and molar mass characteristics of the studied samples

| | |
|---|---|
| Polystyrene latex | |
| Average particle diameter (nm) | 155 |
| Standard deviation of PSD (nm) | 54 |
| Polystyrene | |
| Weight average molar mass (g/mol) | 411000 |
| Number average molar mass (g/mol) | 392000 |

(Rheodyne, USA) with a 1 μl loop and with a system of a graduated micro-splitter valve, model P 470 and a micro-metering valve, model P 446 (Upchurch Scientific, USA) allowing the splitting of the carrier liquid flow into two separated entries of the channel and also the casual splitting of the outgoing liquid between the detector and the waste. A schematic representation of the micro-TFFF unit is shown in Fig. 3. More detailed information concerning the micro-TFFF unit is available on: microfrac@atlas.cz.

An aqueous solution of 0.1% detergent Brij 78 (Fluka, Germany) and 3 mM NaCl was used as one of the carrier liquids. In some cases only the deionized water was used without NaCl and the detergent. The tetrahydrofuran (THF) was used as a carrier liquid for the separation of polystyrene (PS) standard. Various temperature drops $\Delta T$ across the channel and various temperatures of the cold wall $T_c$ were chosen as convenient according to our previous studies. The flow rates (in μl/min) were chosen in such a way to cover the most useful range from the viewpoint of practical applications.

Spherical polystyrene latex (PSL) particles sample (Polymer Laboratories, Great Britain) of narrow particle size distribution (PSD), PS standard of narrow molar mass distribution (MMD) (Waters Ass., USA), and the pure acetone (non-retained marker molecules) were used in this study. The particle size and molar mass characteristics of the PSL and PS samples are given in Table 1.

## 3. Results and discussion

### 3.1. Operating mode of micro-TFFF unit

A scheme of the fluidic circuit of the micro-TFFF unit is shown in Fig. 3. The carrier liquid flow provided by a syringe-type pump is split by the graduated micro-splitter valve into two streams. The first part goes directly to the micro-TFFF channel inlet, the second one, main part, to the injection valve. The sample to be fractionated is injected in the micro-TFFF channel via the second input situated farther from the first inlet in the centre-line of the micro-TFFF channel. In such a manner, the zone of the injected sample does not reach the side walls because the free carrier liquid forms two thin layers that flow at the side walls thus forming a sheath contouring the main central stream.

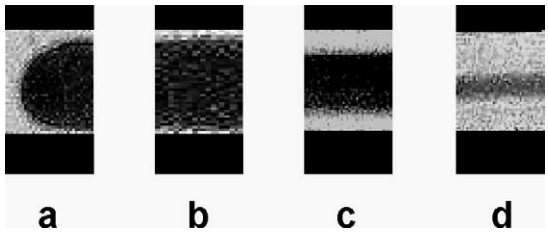


Fig. 4. Macro-photographs of the zones of a dye injected in the central main stream and the uncoloured water layers flowing in the channel edge layers. The splitting ratios were: (a) $s = 0.08$, hemi-circular zone formed at the injection point (b) $s = 0.08$, central part of the zone at some distance from the injection point (c) $s = 0.69$, central part of the zone at some distance from the injection point (d) $s = 3.45$, central part of the zone at some distance from the injection point.

Nearly hemi-circular shape of the injected sample zone formed just at the injection point is shown in Fig. 4a, which is a macro-photograph of a dye injected into the uncoloured water used as a carrier liquid. It has to be stressed that in order to obtain axially symmetrical shape of the sample zone at the injection point and axially symmetrical central main stream, the main upper and lower walls of the channel must be perfectly parallel. This was not rigorously the case shown in macro-photographs in Fig. 4, because the upper wall was made of a soft Plexiglas that was slightly deformed when clamped with the lower main wall of the model micro-channel that served only for the described demonstration of the flow pattern. In our real micro-TFFF channel, its original construction guaranties the perfect parallelism of the main walls. According to the splitting ratio $s$, which is the ratio of the flow rate of the carrier liquid passing directly to the first micro-channel input to that entering the channel via the injection valve, it is possible to control the ratio of the breadth of the main central liquid stream to that of the side wall liquid layers. This is demonstrated in Fig. 4b–d, representing the central main stream (photographed at some distance downstream from the injection point) formed by the injection of a dye at different splitting ratios, roughly $s = 0.08$, 0.69 and 3.45, respectively.

Our previous calculations have shown [9] that the breadth $E$ of the edge layer in Fig. 2 (in which the flow velocity in the plane parallel to the main walls rapidly increases until reaching the central plateau of quasi-constant linear velocity) is roughly equal to the thickness of the channel $w$, independently of the aspect ratio. Consequently, the splitting ratio $s$, necessary to avoid an important penetration of the separated species (flowing in the main central stream) to the

edge layers, must be higher than approximately:

$$s \geq \frac{2E}{b-2E} = \frac{2w}{b-2w} = \frac{2}{a-2} \quad (4)$$

It means that $s$ should not be lower than 0.067 in the case of our above described micro-TFFF channel. All tested splitting ratios shown in Fig. 4, fulfil this condition.

Obviously, the Eq. (4) is an approximation because the ratio of the mean flow rate in the main central stream to that in both edge streams is not simply proportional to the ratio of the corresponding stream breadths as supposed by the Eq. (4). The simplification in Eq. (4) does not take into account the decrease in average linear velocity near the side walls due to the established flow velocity profile in the plane parallel to the main walls. Nevertheless, as far as the splitting ratio to be established by the graduated micro-splitter valve is very difficult to estimate theoretically because the exact hydrodynamic resistances of two separate conduits (including the internal volume of the valve and both capillaries connecting the valve outputs with the micro-channel inputs) are practically impossible to calculate, the only accurate procedure is an experimental calibration of the valve graduation with respect to the optimum splitting ratio.

The modification of the injection mode by the hydrodynamic splitting of the carrier liquid flow into two separate streams made possible another optimization of the micro-TFFF channel design and the simplification of its construction. Usually, the FFF channel (cut in a foil determining its thickness) is equipped with two triangular ends, as can be seen in Fig. 5a. The calculations by conformal mapping procedure published by Williams at al. [15] have shown that an additional band broadening is caused by these ends and that it decreases with decreasing angle of the top of triangular end. An angle of 30° was considered as a reasonable optimum. Our modification of the injection mode does not impose such a shape of the channel ends. Consequently, the hemi-circular ends shown in Fig. 5b were chosen and confirmed experimentally as convenient. The band broadening is not influenced by the shape of the channel ends whenever the main central stream is confined between two edge streams. The confinement of differently coloured liquid streams at the channel outlet without an important mixing has already been demonstrated in our previous paper [11] and is demonstrated again in Fig. 5c and d. Although two ends of the channel in Fig. 5c and d have different but not the hemi-circular shapes, the flow pattern was similar, proving no observable mixing of different streams inside the channel before entering the outlet capillary.

### 3.2. Performance of hydrodynamic splitting injection mode

The performance of the new injection mode, based on the hydrodynamic splitting of the carrier liquid flow entering the micro-TFFF channel, was tested by injecting the non-retained solute (acetone) in pure water at different splitting ratios. Two different thicknesses of the channel

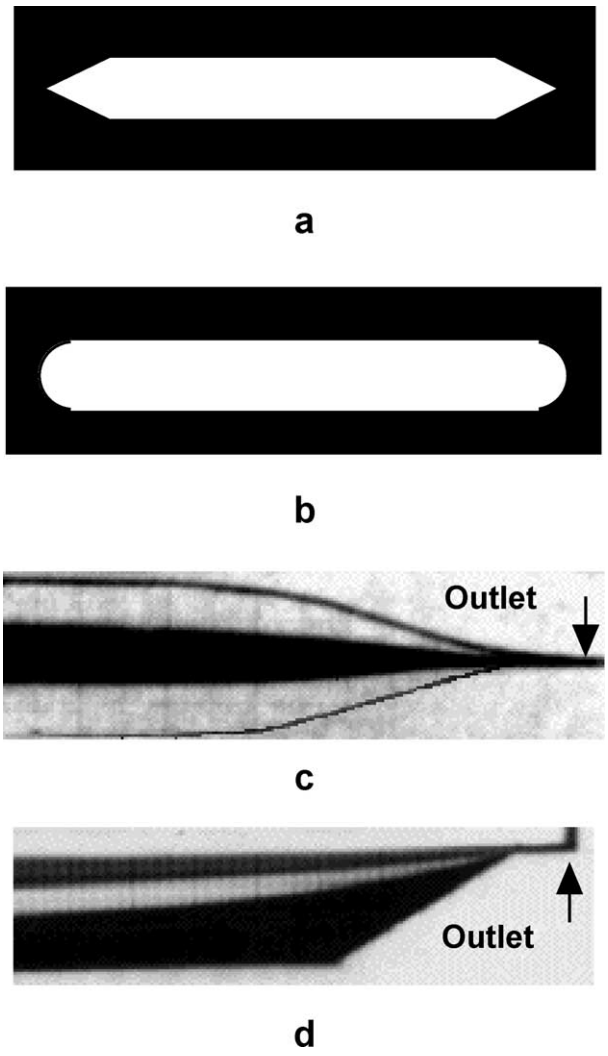


Fig. 5. Schematic representation of different channels equipped with triangular ends (a) or hemi-circular ends (b). The macro-photographs of the zones of a dye injected in the central main stream and the uncoloured water layers flowing in the channel edge layers at the proximity of the channel outlets of different shapes (c and d).

were used, namely $w = 0.100$ and 0.250 mm. The testing was carried out also for a retained PS standard in THF by using the described micro-TFFF unit with the channel of $w = 0.100$ mm and by using the same micro-TFFF unit but equipped with a channel of standard shape with two triangular ends, as shown in Fig. 5b, and $w = 0.100$ mm, both studies carried out under similar experimental conditions. Finally, the comparison was also performed by using our former micro-TFFF channel, model 2003, of different size, namely $w = 0.100$ mm, $L = 96$ mm, and $b = 4.3$ mm.

The experimental results concerning the effect of different splitting ratios on the band broadening of non-retained solute (acetone) are shown in Fig. 6. It can clearly be seen, that the optimal splitting ratio is $s = 0.116$ for the micro-TFFF channel of $w = 0.100$ mm. Higher or lower splitting ratio results in broader zones. More important band broadening which appeared at lower splitting ratio is caused by the

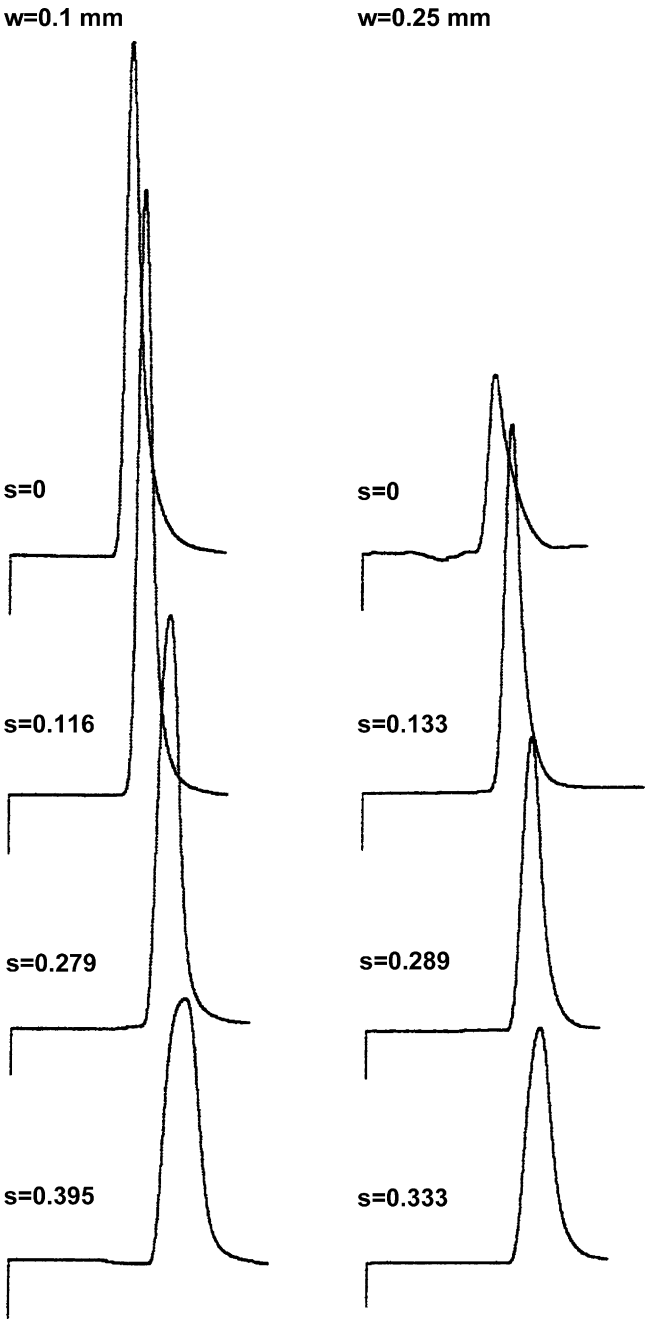


Fig. 6. Fractograms of the acetone obtained at different splitting ratios $s$ in two micro-TFFF channels of different aspect ratios $a$, with $w = 0.100$ mm ($a = 32$) and $w = 0.250$ mm at $\Delta T = 0$ K, $T = 295$ K, and the flow rate 16.67 μl/min, without stop-flow. Carrier liquid: deionized water. The dimensionless elution time axes of all fractograms obtained in channels of different volumes were normalized in order to make the comparison easier.

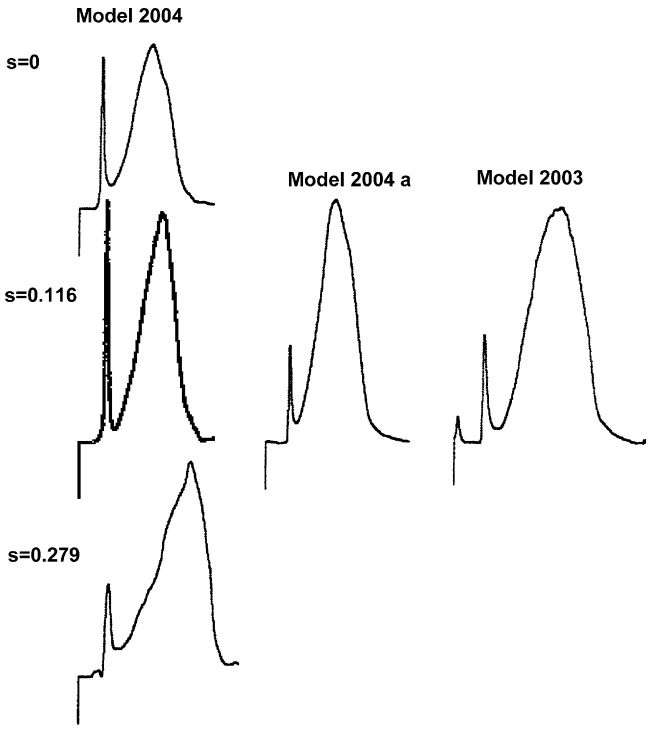


Fig. 7. Fractograms of the PS sample obtained at different splitting ratios $s$ in micro-TFFF channel model 2004 ($w = 0.100$ mm, $a = 32$) under different experimental conditions: flow rate 16.67 μl/min without stop-flow, temperature of the cold wall $T_c = 278$ K, and $\Delta T = 37$ K for $s = 0$ and $s = 0.279$, and $\Delta T = 32$ K for $s = 0.116$. Carrier liquid: tetrahydrofuran. Fractogram of the PS sample obtained in micro-TFFF channel model 2004a ($w = 0.100$ mm, $a = 32$) equipped with standard triangular ends without splitting injection mode under identical experimental conditions as in previous case for $s = 0.116$. Fractogram of the PS sample obtained in micro-TFFF channel model 2003 ($w = 0.100$ mm, $L = 96.5$ mm, $a = 42$) equipped with standard triangular ends without splitting injection mode under the following experimental conditions: flow rate 20 μl/min without stop-flow, temperature of the cold wall $T_c = 278$ K, and $\Delta T = 35$ K. The dimensionless elution time axes of all fractograms obtained in different channels and under different conditions were normalized with respect to the peak position of the unretained species in order to make the comparison easier.

edge effects because the solute molecules can penetrate into the edge layers. On the other hand, an increase in band broadening at higher than optimum splitting ratio is caused by the fact that the same injected volume of the sample, confined in a narrower central stream, is longitudinally more extended and the zone is thus broader. Similar results were obtained with thicker channel ($w = 0.250$ mm), the optimal splitting ratio was, however, somewhat higher, $s = 0.133$. It has to be stressed that the linear velocity of the carrier liquid was roughly 2.5 times lower in thicker ($w = 0.250$ mm) channel in comparison with thinner ($w = 0.100$ mm) channel at the same flow rate (16.67 μl/min). This fact explains almost the same widths of the peaks of acetone in both cases.

The fractograms of the PS standard of molar mass 411 000 g/mol, obtained for different splitting ratios and compared with those obtained with the use of different micro-TFFF channels, are shown in Fig. 7. Here again, the optimal splitting ratio is $s = 0.116$. The fractograms obtained at lower or higher splitting ratios are more broadened. The resolution between the void and polymer peaks is the highest for $s = 0.116$, as can be seen in Fig. 7, regardless the fact that the experimental conditions are slightly less favorable (lower $\Delta T$) for the experiment carried out at $s = 0.116$.

The comparison of the resolutions of the void and retained PS peaks in Fig. 7, obtained with the use of different

micro-TFFF channels, demonstrates clearly, that the best result was achieved with the split-flow mode. The difference between the micro-TFFF channel model 2004 and 2004a is that the former one has a standard shape with two triangular ends and the splitting of the carrier liquid flow was not applied; the sample was injected via the first channel inlet. Regardless the fact that the channel model 2004a was slightly longer, the resolution is lower in comparison with that obtained with the use of model 2004 by applying the split-flow mode injection. The difference in resolutions is not very high but reproducible. The comparison of the resolution obtained with the former channel model 2003 is also in favor of the new micro-TFFF unit equipped with the hydrodynamic splitting option. Moreover, the total heat flow was by some 35% higher in model 2003 micro-TFFF channel in comparison with model 2004 because its aspect ratio was $a = 43$.

### 3.3. Hydrodynamic splitting of outlet stream

The splitting of the outlet streams for sample concentration was originally described by Giddings et al. [16] and applied to sedimentation steric FFF. This concept was later generalized by Giddings [17] and applied several times in some other FFF techniques. The outlet splitting was always realized by a splitter situated at the end of the channel between the accumulation and depletion walls and dividing the outgoing stream of the carrier liquid into the detector and waste capillary. Our construction does not use such a splitter but the splitting is purely hydrodynamic. The micro-metering valve closing the upper outlet capillary (see Fig. 3) allows one to control the splitting ratio of the carrier liquid at the channel outlet. The stream transporting the fractionated species accumulated at one of the main channel walls flows to the detector and the other stream of a pure carrier liquid goes directly to the waste. Thus the outlet splitting ratio can be controlled or the micro-metering valve can be closed if the splitting is undesired, for example in some cases if the focusing is dominating separation mechanism [18]. Nevertheless, it has to be stressed that even if the focusing mechanism is effective, the fractionated species can only exceptionally be present in the depletion half of the channel and thus the outlet splitting ratio $s = 0.5$ can still be applied. Such a situation can appear whenever the lift forces generate the focusing phenomena [18] but the focused zone cannot, in principle, be formed above the central plane parallel to the accumulation wall.

The performance of our outlet hydrodynamic splitting mode was demonstrated by micro-TFFF separation of a PSL sample of the particle diameter 155 nm. The result is shown in Fig. 8. The lower fractogram corresponds to the experiment with the use of the splitting ratio $s = 0$. It means that all outgoing liquid passed through the detector. The higher fractogram corresponds to the splitting ratio $s = 0.5$ which means that a half of the outgoing liquid passed through the detector and the other half was directed to the waste. It can be seen in Fig. 8 that the height of the retained PSL sample increased by the factor 2, correspondingly to the imposed splitting ratio $s = 0.5$. This result confirms that purely hydrodynamic splitting is efficient and thus the construction of the micro-TFFF channel is substantially simplified. It has to be stressed that the ends of the capillaries at the outlet from the detector and at the outlet to the waste should be kept constantly at the same vertical positions in order to keep either zero or the same difference in hydrostatic pressure between them otherwise the splitting ratio cannot be controlled only by the micro-metering valve.

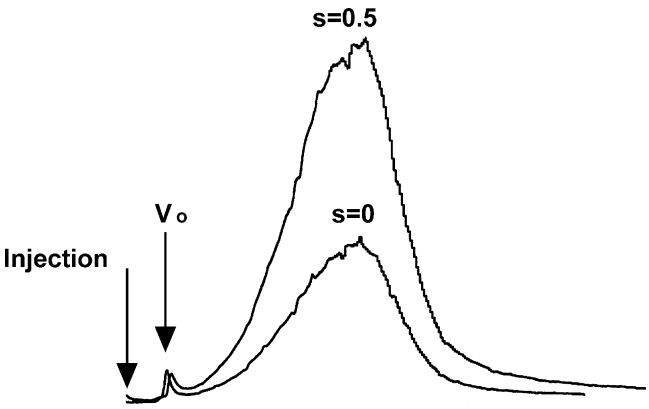


Fig. 8. Fractograms of the PSL latex sample obtained at two different outlet splitting ratios $s = 0$ and $s = 0.5$ in micro-TFFF channel model 2004 ($w = 0.100$ mm, $a = 32$) under the following experimental conditions: flow rate 10 μl/min without stop-flow, temperature of the cold wall $T_c = 311$ K, and $\Delta T = 24$ K, and inlet $s = 0.116$. Carrier liquid: aqueous solution of 0.1% Brij 78 and 3 mM NaCl.

### 3.4. Determination of the sign of Soret coefficient

It has been proposed recently [19] to determine the sign of the Soret coefficient (it means to see whether the retained species migrate to the cold or hot wall) by comparing the retentions in horizontal and vertically positioned channel. Whenever the channel is positioned vertically, the horizontal density gradient causes an upward convective flow at the hot wall and a downward flow at the cold wall. The coupling of this convective flow with the forced unidirectional flow results in a more asymmetrical flow velocity profile compared with the profile formed in horizontal channel. As a result, the mean velocity of a retained zone decreases if the forced flow has an upward direction in the vertical channel and the retained species accumulate at the cold wall in comparison with the mean velocity in the horizontal channel whereas the mean velocity of a retained zone in the vertical channel increases in comparison with the velocity in the horizontal channel for the species accumulated at the hot wall. An increase or decrease of the velocity is inverted with respect to the accumulation walls if the forced flow has a downward direction. The hydrodynamic splitting of the outlet streams allows one to determine the sign of the Soret coefficient even more simply by applying the splitting ratio $s = 0.5$ and by detecting by which outlet the retained species leave the channel. The connection of a detector to any outlet capillary is simple and thus maximum two experiments are enough

to determine at which wall the retained species accumulate. In our case (see Fig. 8), the detector was connected to lower outlet thus the retained species accumulated at the cold wall.

## 4. Conclusion

The original injection mode by the hydrodynamic splitting of the carrier liquid flow into the main central stream and two thin stream layers at the side walls of the channel proved its efficiency to eliminate the edge effects in micro-TFFF channel. The band broadening resulting from the low aspect ratio of a miniaturized TFFF channel is reduced. This construction using the injection valve makes the injection procedure perfectly controllable and reproducible. The hydrodynamic splitting of the outlet streams allowed not only an increase in the concentration of the detected species but also the determination of the sign of Soret coefficient. As a result, high versatility and extended range of the operational variables that can be controlled are achieved with micro-TFFF due to substantially reduced heat flux across the miniaturized channel. The hydrodynamic splitting of the carrier liquid flow contributed to the reduction of the channel aspect ratio without losing the performance of separations.

## References

[1] J. Janča, J. Liq. Chromatogr. Rel. Technol. 25 (2002) 683.
[2] J. Janča, J. Anal. Chim. Acta, in press.
[3] J. Janča, J.-F. Berneron, R. Boutin, J. Colloid Interface Sci. 260 (2003) 317.
[4] J. Janča, I.A. Ananieva, e-Polymer (34) (2003).
[5] J. Janča, I.A. Ananieva, A.Yu. Menshikova, T.G. Evseeva, J. Dupák, J. Chromatogr. A 1046 (2004) 162.
[6] M.J.E. Golay, J. Chromatogr. 216 (1981) 1.
[7] M. Martin, J.-L. Jurado-Baizaval, G. Guiochon, Chromatographia 168 (1982) 98.
[8] J.C. Giddings, J.P. Chang, M.N. Myers, J.M. Davis, K.D. Caldwell, J. Chromatogr. 255 (1983) 359.
[9] J. Janča, M. Hoyos, M. Martin, Chromatographia 33 (1992) 284.
[10] J. Janča, Collect. Czech. Chem. Commun. 68 (2003) 672.
[11] J. Janča, N. Nováková, J. Liq. Chromatogr. 10 (1987) 2869.
[12] J. Janča, N. Nováková, J. Chromatogr. 452 (1988) 549.
[13] J.C. Giddings, M.R. Schure, Chem. Eng. Sci. 42 (1987) 1471.
[14] L.K. Smith, M.N. Myers, J.C. Giddings, Anal. Chem. 49 (1977) 1750.
[15] P.S. Williams, S.B. Giddings, J.C. Giddings, Anal. Chem. 58 (1986) 2397.
[16] J.C. Giddings, H.C. Lin, K.D. Caldwell, M.N. Myers, Sep. Sci. Technol. 18 (1983) 293.
[17] J.C. Giddings, Anal. Chem. 57 (1985) 945.
[18] J. Janča, I.A. Ananieva, A.Yu. Menshikova, T.G. Evseeva, J. Chromatogr. B 800 (2004) 33.
[19] J. Janča, Phil. Mag. 83 (2003) 2045.